Research Article

Shaoli Fu, Xiaohong Chen*, Ping Liu, Honglei Zhou, Fengcang Ma, and Wei Li

Preparation of layered gradient Cu–Cr–Ti alloy with excellent mechanical properties, thermal stability, and electrical conductivity

https://doi.org/10.1515/ntrev-2022-0500
received July 6, 2022; accepted September 15, 2022

Abstract: Cu–Cr–Ti alloy with gradient properties was prepared at 960°C for 2 h in air, 80% cold rolling, and then aging at 500°C for 1 h. The results showed that the surface layer of Cu–Cr–Ti alloy had achieved a good match of electrical conductivity (96.2% International Annealed Copper Standard (IACS)), thermal stability (softening temperature of 650°C), and wear resistance (friction coefficient of 0.17). Meanwhile, the core region maintains high tensile strength (519 MPa) and good electrical conductivity of 71.8% IACS. Transmission electron microscope characterization revealed that the precipitates of surface layer are composed of Cr oxides, complex oxides formed by Cu, Cr, and O, and Ti-rich phases. The existence of oxide particles with discontinuous distribution and stable properties is the reason for the good electrical conductivity, excellent thermal stability, and outstanding wear resistance of the surface layer. The main precipitates of the core are Cr. The high tensile strength of the core is ascribed to the aging strengthening effect of these fine Cr particles. This work provides ideas and approaches for the preparation of copper alloy with excellent properties for high-speed railway contact wire, and solves the drawbacks of composites synthesized from heterogeneous materials.

Keywords: Cu–Cr–Ti alloy, gradient properties, internal oxidation, oxides, fine Cr precipitates

*** Corresponding author: Xiaohong Chen,** School of Materials and Chemistry, University of Shanghai for Science and Technology, Shanghai 200093, China, e-mail: cxhusst@163.com
Shaoli Fu, Ping Liu, Honglei Zhou, Fengcang Ma, Wei Li: School of Materials and Chemistry, University of Shanghai for Science and Technology, Shanghai 200093, China

1 Introduction

With the rapid development of railways, the speed of railway transportation is increasing again and again, and it is about to enter 400 km/h or even higher. The contact line of high-speed railway needs higher conductivity, higher strength, better thermal stability, wear resistance, and so on, but it is difficult to improve the strength and conductivity at the same time [1–3]. In order to obtain the materials that meet the above requirements, some researchers have prepared oxygen-free Cu [4] or single crystal Cu [5–8] by special techniques, whose transmission frequency was greatly improved, but their mechanical properties was very poor. In addition, the skin-effect of high-frequency signals was also studied to synthesize copper [9–13]/aluminum clad steel [14–16] by using steel wire with high tensile strength in the core region and copper/aluminum with excellent electrical conductivity in the surface layer. However, many impurities and lattice defects will inevitably be introduced during the process of preparation, which were distributed at the interface between copper/aluminum and steel, affecting the bonding strength between them. Furthermore, the presence of impurities and defects will reduce the effect of signal transmission. And simultaneously due to the great difference in mechanical and physical properties between copper/aluminum and steel, there is a great difference in deformability between the two metals, which will also affect their bonding strength and ultimately weaken the excellent properties of copper/aluminum clad steel. Besides, it was reported that a nanostructured supersaturated solid solution of Cu–Cr alloy was prepared by combining the mechanical alloying and spark plasma sintering, and the high temperature mechanical properties have been greatly improved, but the electrical conductivity is only about 60% International Annealed Copper Standard (IACS) [17]. In addition, the tensile strength of another Cu–Cr alloy with up to 80% IACS is less than 500 MPa [18,19]. And the comprehensive

properties of Cu–Cr–Ti prepared by traditional heat treatment and deformation cannot meet the application requirements of the contact line of high-speed railway [20–22].

Therefore, the aim of this work is to prepare a Cu alloy with excellent comprehensive properties, to achieve high electrical conductivity on the surface and high strength in the core in a single alloy, to achieve a perfect combination of higher electrical conductivity and higher strength, to solve the drawbacks of composites synthesized from heterogeneous materials. The Cu–Cr–Ti alloy was treated by the combinational process of internal oxidation [23], cold rolling, and aging. The traditional internal oxidation process requires a medium to supply oxygen, such as the commonly used Cu_2O [24,25]. In this work, the internal oxidation only needs to be carried out under the atmosphere of air, so the process is simple and easy to operate. Moreover, Ti can delay the growth of precipitates and improve the mechanical properties of the alloy [26]. In addition, since the solid solubility of Cr in Cu at high temperature is only 0.65 wt% [27], even if the Cr remains in the Cu matrix that is not internally oxidized, it can be easily precipitated by the subsequent heat treatment [28–30]. Hence, the electrical conductivity of Cu–Cr–Ti alloy is greatly improved, and the Cr oxide particles precipitated on the surface layer greatly improve the thermal stability and wear resistance. At the same time, the fine Cr particles precipitated on the core play an aging strengthening role on the matrix, so that the surface layer achieves a good match of electrical conductivity, thermal stability, and wear resistance, while the core ensures the strength. More importantly, owing to the continuous distribution of the atomic lattice at the interface between the surface and the core region, the interfacial bonding is strong, and the interface is pure without impurities.

2 Experimental

The composition of the Cu–Cr–Ti alloy used in this experiment was 0.34 wt% Cr and 0.066 wt% Ti. And the as-cast Cu–Cr–Ti alloy can be obtained by the following steps: first, the A-grade electrolytic Cu was put into the crucible, next Cu–25% Cr was added after the electrolytic Cu melted completely, then Cu–22% Ti alloy was added after holding for 5 min; meanwhile, the temperature was raised and held for 10 min and at last cast for molding (the casting temperature was controlled at about 1,400°C). Subsequently, it was treated by the internal oxidation process. The atmosphere was air containing 20.8% O_2, the temperature was 960°C, and the time was 2, 4, 6, 8, 10, and 12 h, respectively. In particular, the part that was internal oxidized was denoted by ITOX, and the rest was considered to have undergone solution treatment, which was denoted by ST. Then, it was subjected to 80% deformation and aging treatment at 500°C for 1 h under the atmosphere of Ar. The samples after aging treatment were represented by ST + 80% + aging and ITOX + 80% + aging, respectively. The internal oxidation and aging treatment were performed in a tube furnace with a pipe diameter of 80 mm (OTF-1200X, Hefei Kejing material technology Co., Ltd, China). The whole process flow is shown in Figure 1.

The hardness was tested by a Vickers hardness tester (HVS-1000Z, Shanghai Juhui Instrument Manufacturing

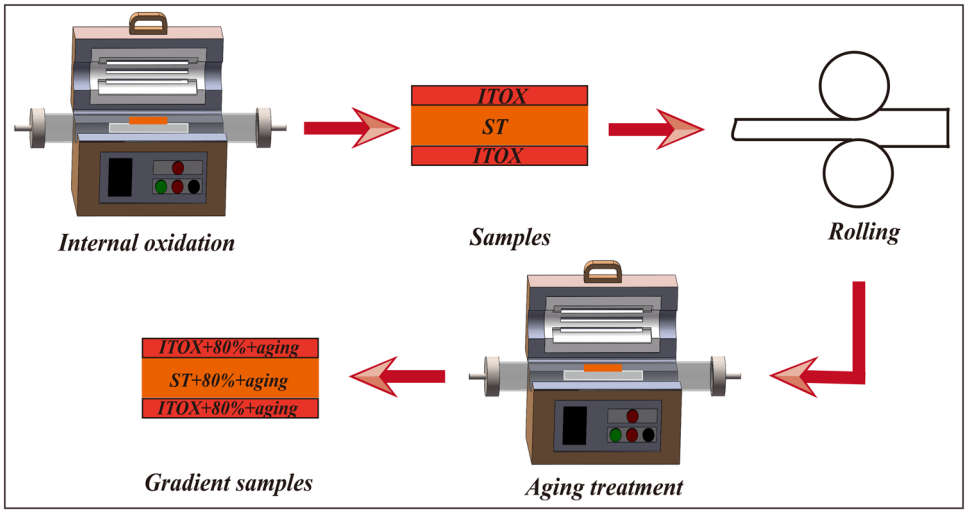

Figure 1: The process flow of the Cu–Cr–Ti alloy.

Co., Ltd, China) under 200 g load for 15 s. The electrical conductivity was assessed by a digital metal electrical conductivity tester (D60K, Xiamen Xinbot Technology Co., Ltd, China). The friction coefficient was measured by a reciprocating friction-wear tester (HSR-2M, Lanzhou Zhongke Kaihua Technology Development Co., Ltd China). The tensile properties were measured by a 50 kN universal testing machine (X050, Zwick Corporation, Germany) at room temperature. Remarkably, in order to complete tensile test, wear test and other of the ST and ITOX samples, Cu–Cr–Ti alloy was treated at 960°C for 12 h in air. Then we can get a materials with the internal oxidation layer of 1.3 mm, 1.3 mm was regarded as ITOX, and the remaining part was ST. The two parts were subjected to the corresponding tests. The scanning electron microscope (SEM, Quanta FEG 450, FEI, USA) was adopted to observe the friction-wear morphologies and hardness indentation. Transmission electron microscope (TEM, Tecnai G2 F30, FEI, USA) was utilized to characterize the micro- and nano-scale structural morphologies. Energy Disperse Spectroscopy (EDS) was used to analyze the composition of the precipitates. In addition, it should be pointed out that the hardness and tensile strength of Cu–Cr–Ti alloy treated only by ST or ITOX were low, which cannot meet the requirements of practical use, so the softening temperature and tensile strength of the two states were not discussed.

3 Results

3.1 Effect of internal oxidation time on the properties of Cu–Cr–Ti alloy

Figure 2(a) shows the thickness of the internal oxidation layer against time. The thickness increased with the

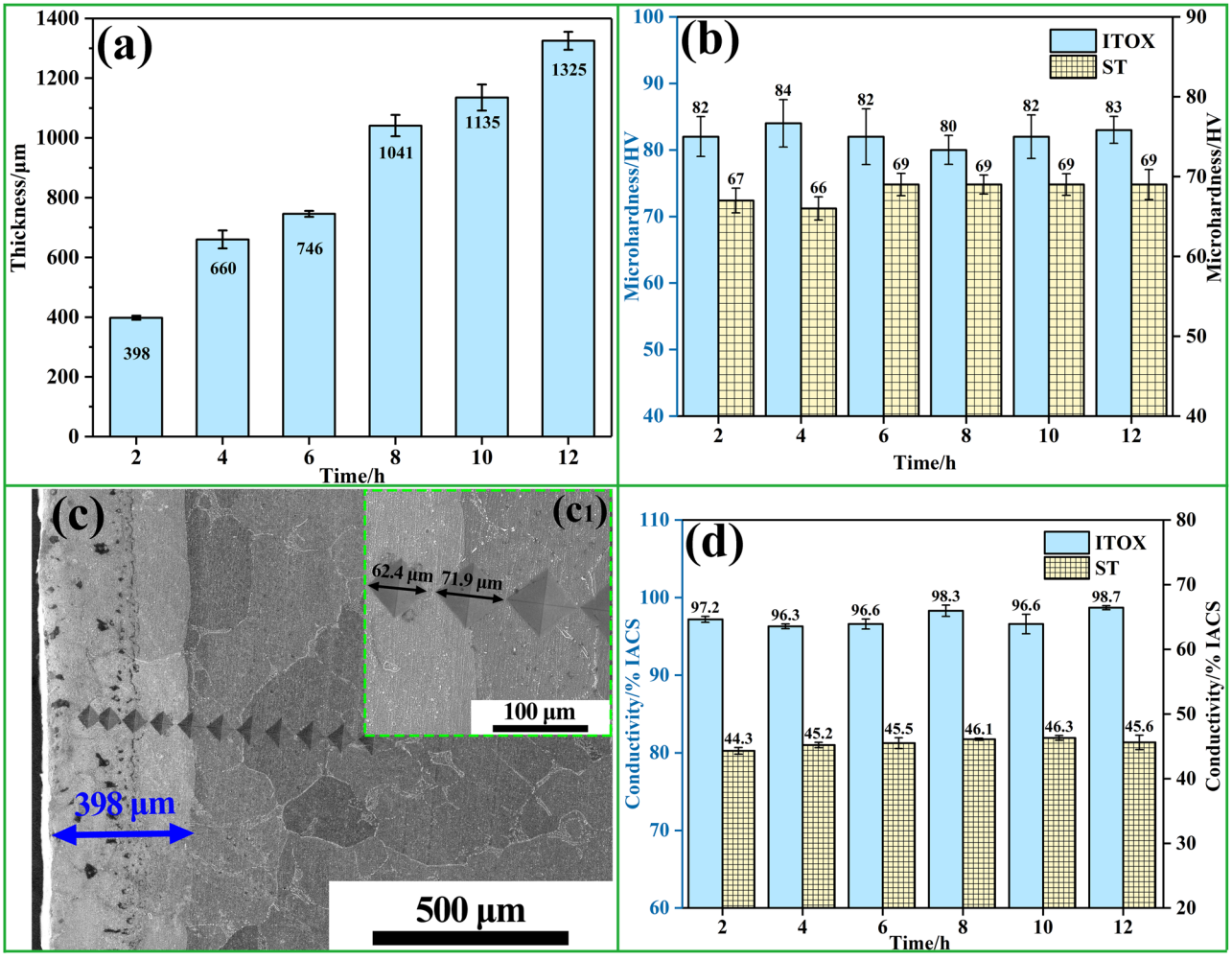

Figure 2: (a) Effect of internal oxidation time on the thickness; (c) microhardness indentation image of Cu–Cr–Ti alloy; (b) microhardness and (d) electrical conductivity of Cu–Cr–Ti alloy after ST and ITOX treatment for different time.

prolonging of time. The reason was that the decrease in the diffusion activation energy of Cr atoms in the Cu lattice made it easier for oxygen atoms to penetrate into the interior through the surface, so the depth of the internal oxidation layer increased gradually. Therefore, we can control the thickness of the internal oxidation layer by controlling the time. As shown in Figure 2(b), the microhardness of ST was about 68 HV, and it was significantly increased to about 82 HV after the internal oxidation treatment. The reason was that Cr has a strong affinity for O [31], which made Cr gradually precipitate from the Cu matrix, forming stable and dispersed strengthening phase particles, hindering the movement of dislocations and greatly improving its hardness [32]. Figure 2(c) is the microhardness indentation image of the sample treated at 960°C for 2 h, and the blue arrow is marked as the internal oxidation layer. It can be clearly seen from the inset c_1 that when the microhardness indentation transited from the ITOX to the ST layer, the size of the indentation suddenly increased from 62.4 to 71.9 μm, that is, the hardness decreased.

Figure 2(d) displays the electrical conductivity of ITOX and ST states, which varies with internal oxidation time. The electrical conductivity of ITOX reached above 96% IACS compared with the 45% IACS for ST. Moreover, the internal oxidation time had almost no effect on the conductivity. This was because the Cr and Ti elements were dissolved in the Cu matrix for ST, and the existence of solid solution atoms distorted the lattice of Cu, which increased the probability of electron scattering, leading to a decline in the electrical conductivity. During the process of internal oxidation, the Cr atoms dissolved in the Cu matrix had a strong affinity for O atoms, and Cr was oxidized and gradually precipitated from the Cu matrix, resulting in an increase in electrical conductivity.

3.2 Electrical conductivity and tensile strength of Cu–Cr–Ti alloy

Figure 3(a) shows the stress–strain curves of Cu–Cr–Ti alloy after being treated by ST + 80% + aging and ITOX + 80% + aging. The electrical conductivity and tensile strength are shown in Figure 3(b). It can be seen from Figure 3(a) that the elongation after ITOX + 80% + aging treatment can reach about 20%, which was better than the elongation of 7.5% after ST + 80% + aging treatment. However, its tensile strength (342 MPa) was far lower than that of ST + 80% + aging (519 MPa), and the electrical conductivity of 96.2% IACS for ITOX + 80% + aging was much higher than that of 71.8% IACS for ST + 80% + aging, as shown in Figure 3(b). The reason for this phenomenon is that the size of the precipitates after ST + 80% + aging is smaller than ITOX + 80% + aging, making the tensile strength of the former higher owing to the effect of stronger precipitation strengthening. But meanwhile, the effect of fine precipitates on electron scattering is greater, so the electrical conductivity of the latter is better than that of ST + 80% + aging.

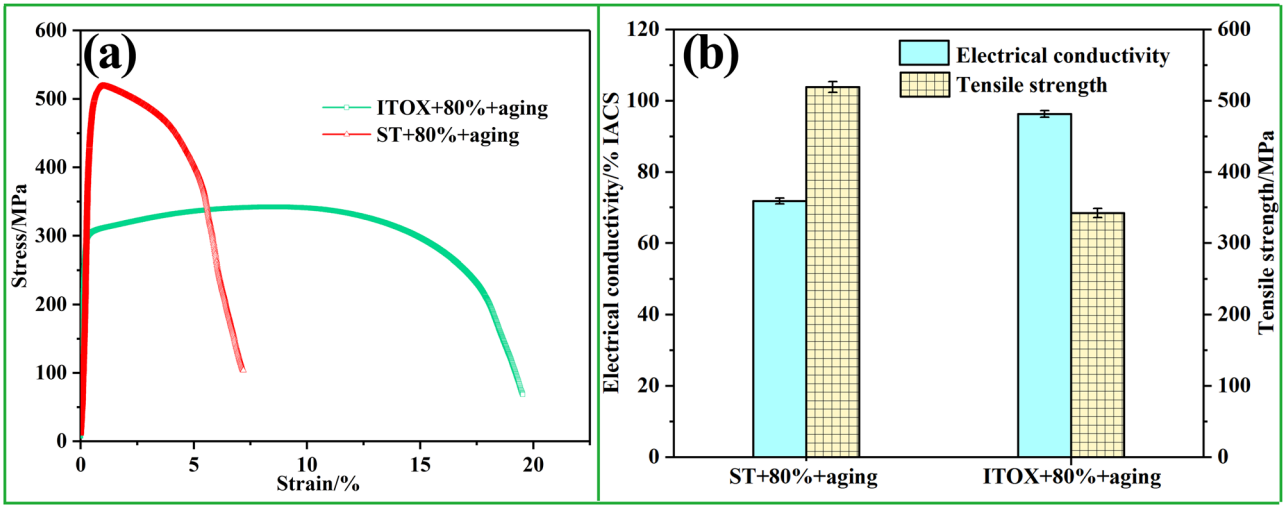

Figure 3: (a) Stress–strain curves and (b) electrical conductivity and tensile strength of Cu–Cr–Ti alloy after being treated by ST + 80% + aging and ITOX + 80% + aging.

3.3 Softening resistance of Cu–Cr–Ti alloy

Figure 4 shows the microhardness of Cu–Cr–Ti alloy varied with temperature after being treated by ST + 80% + aging and ITOX + 80% + aging. As displayed in Figure 4, the microhardness decreased slowly when the temperature was lower than 500°C, and the downturn trend became faster after the temperature was higher than 500°C. And the downturn speed of ST + 80% + aging was faster than that of ITOX + 80% + aging. When the temperature was 568°C, the hardness of the ST + 80% + aging state was 132 HV, which dropped to 80% of the original hardness of 166 HV, so its softening resistance temperature was 568°C. When the temperature was 578°C, the hardness for two states were equal. When the temperature was lower than 578°C, the hardness of ST + 80% + aging was higher than that of ITOX + 80% + aging. But as the temperature continued to rise, the hardness of ST + 80% + aging was lower than that of ITOX + 80% + aging. When the annealing temperature was 650°C, the hardness of the ITOX + 80% + aging state was reduced to 108 HV (80% of the initial hardness of 136 HV), so its softening temperature was 650°C, which was higher than that of ST + 80% + aging. This was because the oxides formed by internal oxidation have more stable properties and stronger ability to resist softening.

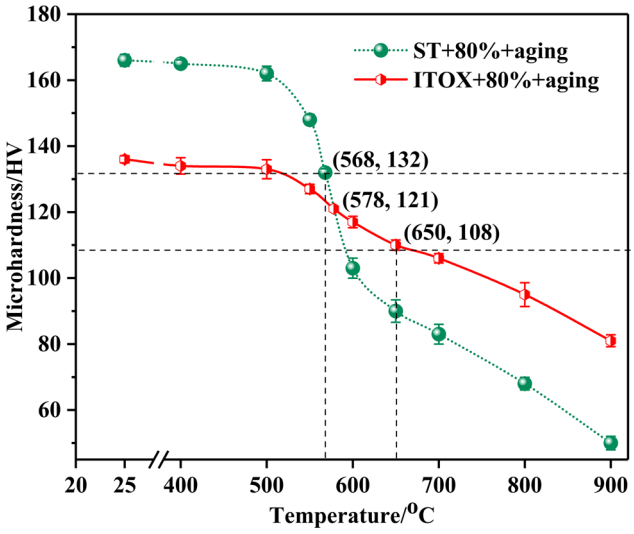

Figure 4: Microhardness of Cu–Cr–Ti alloy after treated by ST + 80% + aging and ITOX + 80% + aging.

3.4 The friction properties of Cu–Cr–Ti alloy

Figure 5(a) and (b) shows the friction coefficient and microhardness of Cu–Cr–Ti alloy after being treated by ST, ITOX, ST + 80% + aging, and ITOX + 80% + aging, respectively. The friction coefficient of ST fluctuated greatly in the initial stage, which can be explained as the polishing process during the wear test, and it finally stabilized at about 0.9. The formation of oxide particles during the ITOX process enhanced the hardness of the Cu matrix (as shown in Figure 5(b)), making the ability of failure resistance improve, that is, its wear resistance improved. Therefore, the friction coefficient of the ITOX

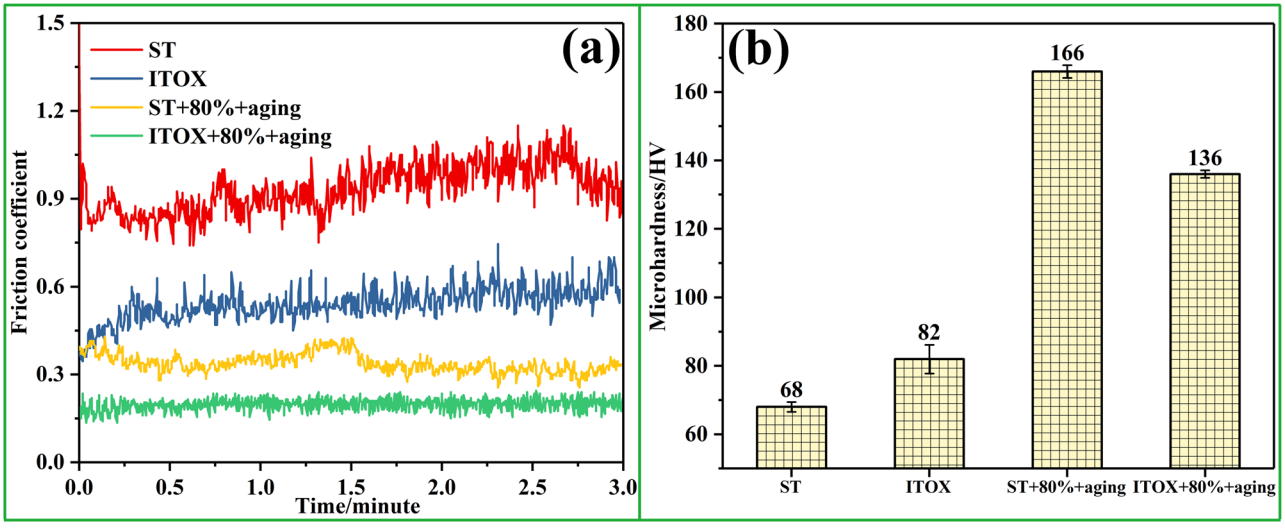

Figure 5: Friction coefficient (a) and microhardness (b) of Cu–Cr–Ti alloy after being treated by ST, ITOX, ST + 80% + aging, and ITOX + 80% + aging.

was smaller than that of the ST. Moreover, the friction coefficient of the ST + 80% + aging (the yellow curve) and ITOX + 80% + aging (the green curve) was reduced compared with those of ST and ITOX. This was due to the fact that fine and dispersed second phase particles will precipitate from the matrix after aging, which will produce a significant strengthening effect on the matrix, making the hardness increase dramatically, as shown in Figure 5(b). The oxide particles formed by internal oxidation had better stability, so the friction coefficient of ITOX + 80% + aging treatment was the smallest and the wear resistance was the best.

Figure 6 shows the SEM images of the friction-wear morphologies of Cu–Cr–Ti after being treated by ST, ITOX, ST + 80% + aging, and ITOX + 80% + aging. As shown in Figure 6(a), since the hardness of ST was low, the hard spots moved on the soft matrix during the friction and wear process, so the surface wear was very serious, and there were a lot of peeling fragments accompanying the formation of chipping pits and grooves, and their wear mechanisms were delamination and adhesive wear. As shown in Figure 6(b), the phenomenon of debris peeling became weaker, and there was a furrow formed by squeezing and scraping against the grinding ball. The main wear mechanism was abrasive wear and weak delamination wear. After ST + 80% + aging, the hardness of Cu–Cr–Ti alloy was greatly improved due to the precipitation of dispersed Cr and deformation strengthening. A small amount of exfoliated fragments and grooves formed by spalling were observed on the worn surface, and the wear mechanism was mainly delamination wear, as shown in Figure 6(c). It can be seen from Figure 6(d) that the worn surface of Cu–Cr–Ti alloy after ITOX + 80% + aging treatment was the smoothest, only a weak furrow phenomenon was observed on the worn surface, and the wear mechanism was abrasive wear.

According to the above analysis, the Cu–Cr–Ti alloy treated by ITOX + 80% + aging has higher electrical conductivity, excellent softening resistance, and better wear resistance, while the part treated by ST + 80% + aging has higher tensile strength and hardness. And the properties of Cu–Cr–Ti are superior to the reported Cu-Gd_2O_3 gradient composites [33], copper/bronze laminates [34], and gradient structured Cu [35]. The diagrammatic drawing of Cu–Cr–Ti gradient alloy is shown in Figure 7. The thickness of the internal oxide layer can be controlled by adjusting the internal oxidation time. Finally, we can prepare the materials with gradient properties, the

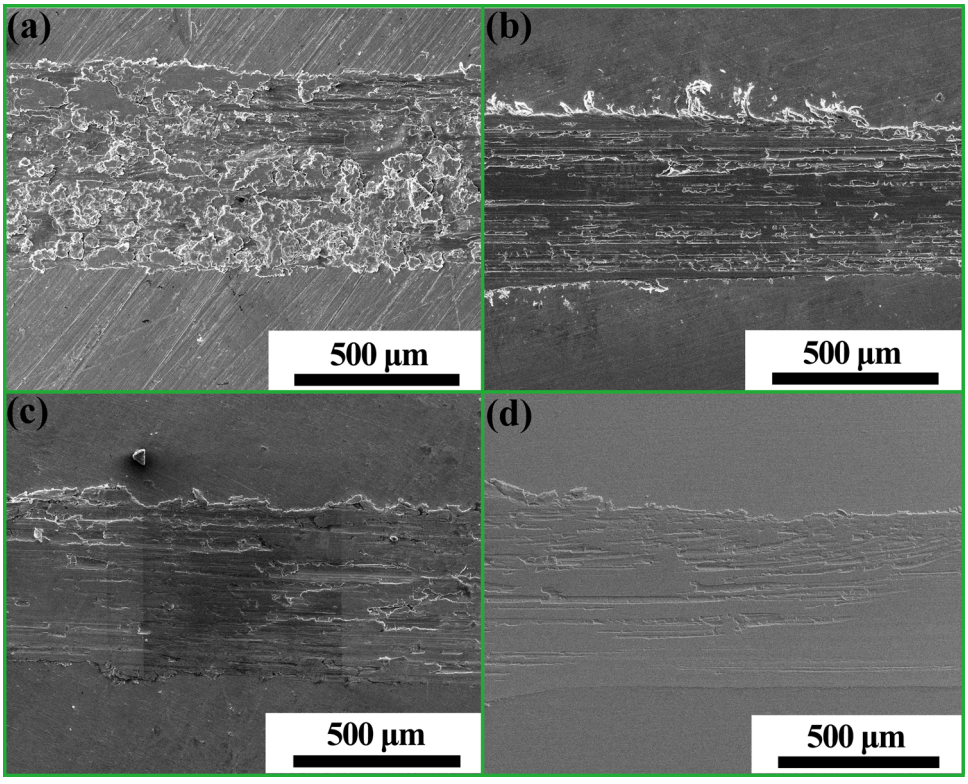

Figure 6: SEM images of the friction-wear morphologies of Cu–Cr–Ti after being treated by (a) ST, (b) ITOX, (c) ST + 80% + aging, and (d) ITOX + 80% + aging.

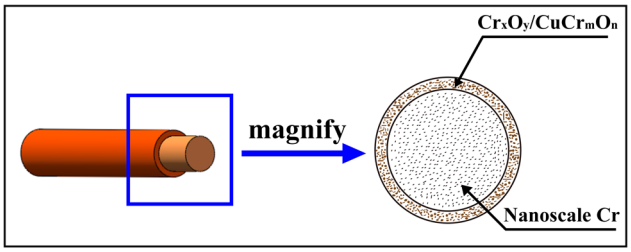

Figure 7: Diagrammatic representation of the prepared Cu–Cr–Ti gradient alloy.

surface layer has good electrical conductivity, excellent wear resistance, and high softening resistance, and the core region has high strength to meet the requirements of high-speed rail contact line.

4 Discussion

According to the above experimental results, there is a great difference in the performance of ITOX + 80% + aging and ST + 80% + aging, so it is necessary to study the specific form of precipitates. For the region treated by ITOX + 80% + aging, 80% cold rolling and aging treatment did not change the existence form of the precipitates. Hence only the existence form of the particles by ITOX was analyzed.

Figure 8 illustrates the TEM images of Cu–Cr–Ti alloy after ITOX treatment. From the bright field image of Figure 8(a) and the dark field image of Figure 8(b), it can be seen that there were rhomboid (circle A), short rod-like (circle B), and rod-like (circles C and D) precipitates in the Cu–Cr–Ti alloy. In order to study these precipitates, high-resolution observation, selected area electron diffraction (SAED), and EDS were carried out on the particles A, B, C, and D. From Figure 8(c), the rhomboid particles mainly contain Cu, Cr, and O elements, and their size was about 47 nm. The inset c_1 and c_2 showed that the particles were composed of $CuCrO_4$ particles with orthorhombic structure, cubic Cu_2O particles, and rhombohedral Cr_2O_3 particles. $CuCrO_4$ (221), Cr_2O_3 (006), and Cu_2O (200) crystal planes overlapped to form the interface among each other, which was parallel to the Cu (002) [31,36]. As displayed in Figure 8(d), the short rod-like particles mainly contain Cu, Cr, O, and Ti elements. The inset d_1 showed that the width was about 13 nm. The inset d_2 proved that the short rod-like precipitate contained $CuCrO_2$ (rhombohedral), Cr_5O_{12} (orthorhombic), Cu_4Ti_3 (tetragonal), and Cu_2O (cubic) particles. And the interface between these particles and the Cu matrix was parallel to the Cu {111}. Figure 8(e) and (f) shows the morphologies of two rod-shaped precipitates with different size. Figure 8(e) showed that the width of the particles C was about 16 nm, and the EDS analysis showed that the main elements were Cu, Cr, and O, and it was the co-phase of $CuCrO_4$ and Cr_2O_3. The width of the particles in Figure 8(f) was about 8 nm. EDS analysis showed that the main elements were Cu, Cr, O, and Ti, and the main phases were $CuCrO_2$ and Cu_4Ti_3.

Based on the above analysis, we can conclude that the precipitates were the coexisting phases of different oxide particles or Ti-rich phases. This was because Cr had a higher chemical affinity for O than Cu, so Cr was easy to form dispersed nano-sized Cr_xO_y and $CuCr_mO_n$ particles in Cu matrix. The existence of these fine and hard particles with good thermal and chemical stability enhanced their ability to resist softening. Meanwhile they can nail dislocations, making dislocations multiply rapidly, which greatly increased the dislocation density, hindered the movement of dislocations, grain boundaries, and sub-grain boundaries. Moreover, they can inhibit static and dynamic recrystallization, so the hardness of ITOX was higher than that of ST. In addition, the Cr element was dissolved in the Cu matrix for ST, which distorted the lattice of Cu matrix, and increased the probability of electron scattering, thereby reducing the electrical conductivity. As a result, the electrical conductivity of the ST samples was very low. During the process of internal oxidation, the Cr atoms gradually precipitated from the Cu matrix for ITOX, so the electrical conductivity of ITOX was much higher than that of ST. The subsequent deformation and aging treatment greatly increased the dislocation density of the Cu–Cr–Ti alloy, so the mechanical properties were improved. For the part treated by ST + 80% + aging, due to the precipitation of Cr atoms from Cu matrix, its conductivity was greatly improved compared with ST. While for the part treated by ITOX + 80% + aging, since most of the Cr atoms have formed stable Cr_xO_y and $CuCr_mO_n$, that is, they have precipitated from the matrix during the internal oxidation, its conductivity has almost no change compared with ITOX.

Figure 9 displays the TEM images of Cu–Cr–Ti alloy after the ST + 80% + aging treatment. The dark field image of Figure 9(b) shows that the fine dispersed precipitates (bright spots) were present in the matrix after aging treatment, and the size ranged from 3 to 7 nm, which was smaller than that of oxides formed by ITOX + 80% + aging treatment. Figure 9(c) is the SAED pattern of the area A in Figure 9(a), the calibration showed that the precipitates were bcc Cr. Compared with the ST, the

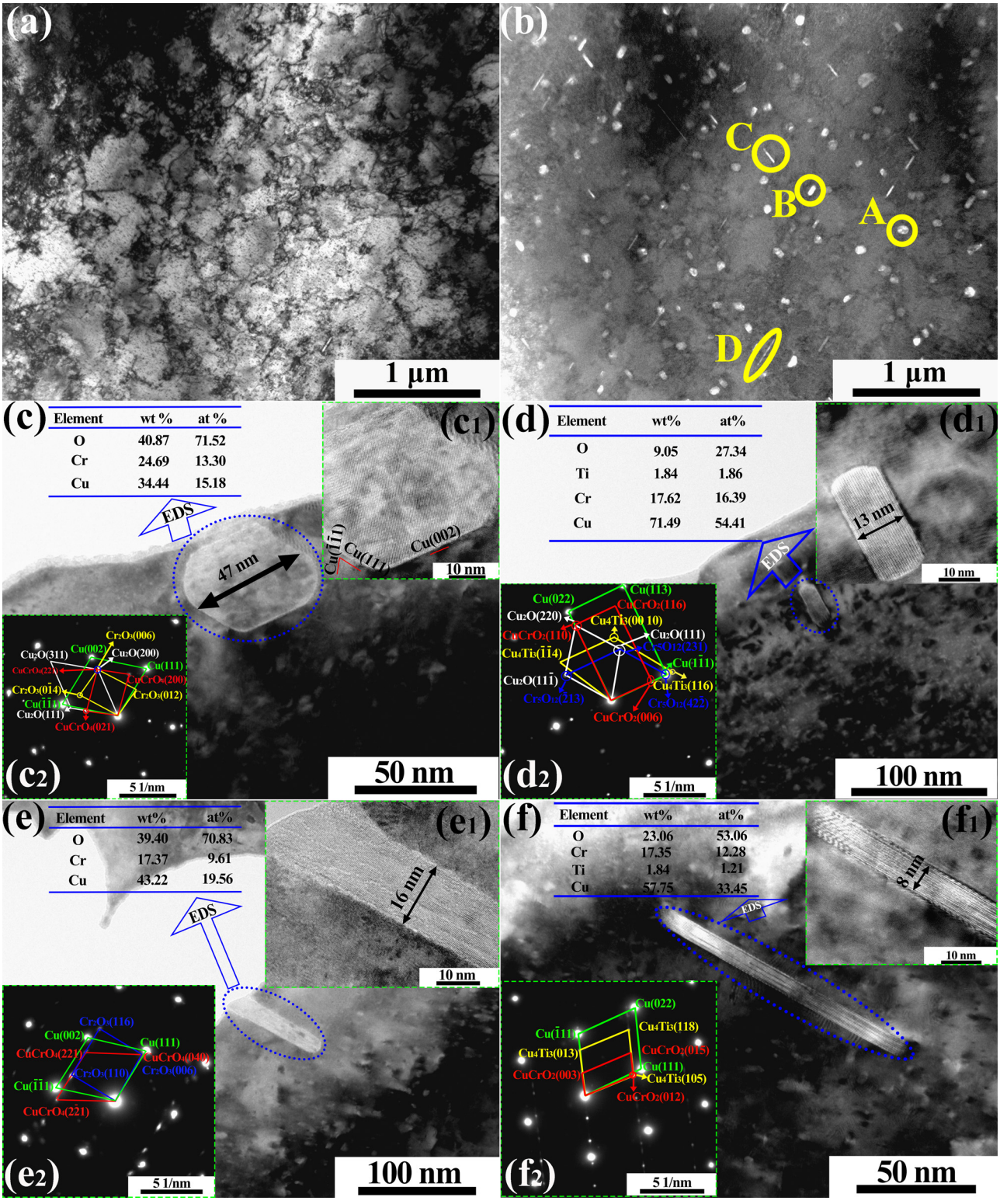

Figure 8: TEM images of Cu–Cr–Ti alloy after ITOX treatment: (a) bright field image; (b) dark field image; (c, d, e and f) the enlarged images; (c_1), (d_1), (e_1) and (f_1) high resolution TEM images inset; (c_2), (d_2), (e_2) and (f_2) SAED pattern of particles A, B, C, and D in (b).

precipitation of Cr improved the tensile strength and electrical conductivity of Cu–Cr–Ti alloy after the ST + 80% + aging treatment.

We can conclude that the main strengthening mechanism of ST + 80% + aging and ITOX + 80% + aging is the precipitates strengthening, so the theoretical calculation

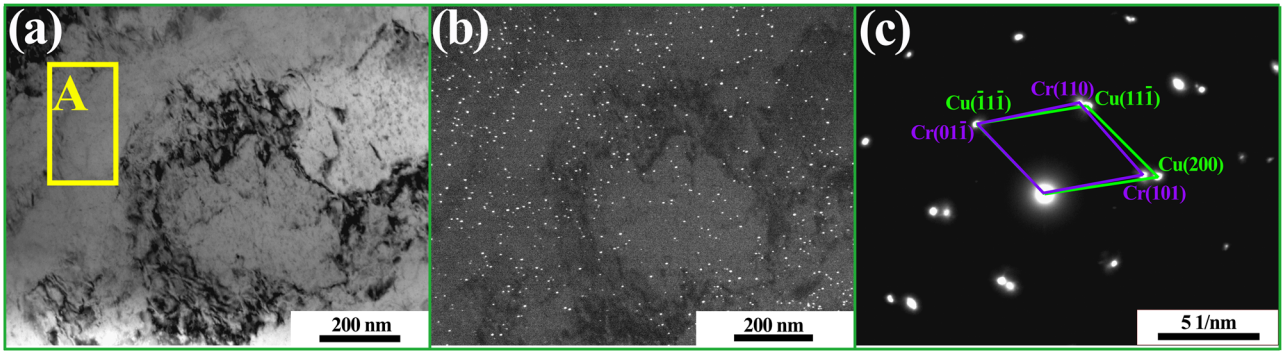

Figure 9: TEM images of Cu–Cr–Ti alloy after the ST + 80% + aging treatment: (a) bright field image; (b) dark field image; (c) SAED pattern of the area A in (a).

is very important to support the experimental results. The main contributions of precipitation strengthening are coherent strengthening and orowan strengthening, and ST + 80% + aging is coherent strengthening, while ITOX + 80% + aging enhancement is mainly orowan strengthening. The main improved strength for ST + 80% + aging and ITOX + 80% + aging can be expressed as the following equations [37,38]:

$$\Delta\sigma_{\mathrm{ST}} = \frac{2.6M(G\beta)^{\frac{3}{2}}}{\sqrt{\frac{dV_f b}{2F}}}, \tag{1}$$

$$F = \alpha G b^2, \tag{2}$$

$$\Delta\sigma_{\mathrm{ITOX}} = \frac{0.4MGb\ln\frac{d}{b}}{\pi\lambda\sqrt{1-\nu}}, \tag{3}$$

$$\lambda = \frac{d\sqrt{\frac{2.093}{v_f}}}{2} - 0.0785d, \tag{4}$$

where M (3.06) is Taylor index, G (42.1 GPa) is the shear modulus of the Cu matrix, b (0.2556 nm) is the Burgers vector, β (0.015) is the mismatch strain constant, d and V_f are the average size and volume fraction of the precipitates, F is the tension of the pinning dislocations of the second-phase, α (0.3) is the geometric parameter, ν (0.34) is the Poisson's ratio, λ is the distance between the precipitates. The increment in strength for ST + 80% + aging and ITOX + 80% + aging strengthening are 209 and 90 MPa, respectively, which are in good agreement with the experimental results.

Figure 10 presents the XRD patterns of the Cu–Cr–Ti alloy of ST + 80% + aging and ITOX + 80% + aging. There were only Cu peaks and no secondary phases after ST + 80% + aging treatment, the reason was that the peak intensity of the precipitates was too weak to detect. Hence, they were covered by the strong peaks of the Cu matrix. The small angle diffraction of the black ellipse proved that there were $CuCrO_2$ (012) peaks in addition to Cu after ITOX + 80% + aging treatment, but no peaks of Cr and Cu oxides were present, indicating that the nano-precipitates after internal oxidation treatment were mainly complex oxides formed by Cu, Cr, and O.

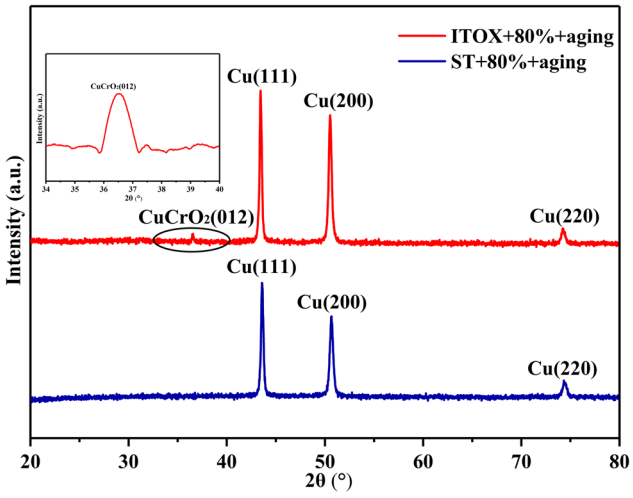

Figure 10: XRD patterns of the Cu–Cr–Ti alloy of ST + 80% + aging and ITOX + 80% + aging.

5 Conclusion

1) With the increase in internal oxidation time, the thickness of the internal oxidation layer increases gradually, and the electrical conductivity (above 96% IACS) and hardness (82 HV) of the ITOX region are much higher than those of the ST region (45% IACS and 68 HV).
2) After 80% deformation and aging at 500°C for 1 h, the Cu–Cr–Ti alloy exhibits obvious gradient properties.

The surface area has an electrical conductivity of 96.2% IACS, a softening temperature of 650°C, a tensile strength of 342 MPa, and a friction coefficient of 0.17, while the core region has a tensile strength of 519 MPa, an electrical conductivity of 71.8% IACS, and a softening temperature of 568°C.

3) The precipitates of the surface layer are Cr oxides, the complex oxides formed by Cu, Cr, and O, and the Ti-rich intergrowth phases, while the precipitates of the core are finely dispersed Cr.

Funding information: This work was supported by the Shanghai Engineering Research Center of High-Performance Medical Device Materials (No. 20DZ2255500), the National Key R&D Program of China (Grant No. 2017YFB0306405), the State Key Laboratory of Advanced Optical Communication Systems and Networks (Grant No. 2018GZKF03007), and the National Natural Science Foundation of China (Grant No. 51201107).

Author contributions: All authors have accepted responsibility for the entire content of this manuscript and approved its submission.

Conflict of interest: The authors state no conflict of interest.

References

[1] Jia SG, Liu P, Ren FZ, Tian BH, Zheng MS, Zhou GS. Sliding wear behavior of copper alloy contact wire against copper-based strip for high-speed electrified railways. Wear. 2007;262:772–7.

[2] Liu Q, Zhang X, Ge Y, Wang J, Cui JZ. Effect of processing and heat treatment on behavior of Cu–Cr–Zr alloys to railway contact wire. Metall Mater Trans A. 2006;37A(11):3233–8.

[3] Jia SG, Liu P, Ren FZ, Tian BH, Zheng MS, Zhou GS. Electrotribological behavior of Cu-Ag-Zr contact wire against copper-base strip. Met Mater Int. 2005;11(1):71–6.

[4] Ghosh G, Sidpara A, Bandyopadhyay PP. Experimental and theoretical investigation into surface roughness and residual stress in magnetorheological finishing of OFHC copper. J Mater Process Tech. 2021;288:1–13.

[5] Soda H, Mclean A, Wang Z, Motoyasu G. Pilot-scale casting of single-crystal copper wires by the Ohno continuous casting process. J Mater Sci. 1995;30(21):5438–48.

[6] Chen J, Yan W, Wang XY, Fan XH. Microstructure evolution of single crystal copper wires in cold drawing. Sci China Ser E:Tech Sci. 2007;50(6):736–48.

[7] Chen J, Yan W, Chen SK, Wang XY, Peng YL, Fan XH. Substructure formed in cold drawn processing for single crystal copper wires. Rare Met Mat Eng. 2007;36(11):1896–900.

[8] Chen J, Yan W, Miao J, Peng YL, Fan XH. TEM analysis of drawn single crystal copper wires produced by OCC method. Rare Met Mat Eng. 2011;40(10):1727–31.

[9] Li HJ, Ding ZM, Chen ZG, Tan FL, Wu JW. Evolution of grain orientation and texture of copper and steel in copper cladding steel wires during drawing and annealing. Mater Res Express. 2019;6(10):218–23.

[10] Liu BX, Wei JY, Yang MX, Yin FX, Xu KC. Effect of heat treatment on the mechanical properties of copper clad steel plates. Vacuum. 2018;154:250–8.

[11] Sasaki TT, Barkey M, Thompson GB, Syarif Y, Fox D. Microstructural evolution of copper clad steel bimetallic wire. Mat Sci Eng A-struct. 2011;528(6):2974–81.

[12] Ko DC, Lee SK, Kim BM, Jo HH, Jo H. Evaluation of copper coating ratio in steel/copper clad wire drawing. J Mate Process Tech. 2007;186(1):22–6.

[13] Li H, Ding Z, Zhao R. Interfacial microstructure and its influence on resistivity of thin layers copper cladding steel wires. Phys Met Metallogr. 2018;119(4):332–8.

[14] Jin JY, Hong SI. Effect of heat treatment on tensile deformation characteristics and properties of Al3003/STS439 clad composite. Mat Sci Eng A-struct. 2014;596:1–8.

[15] Akramifard HR, Mirzadeh H, Parsa MH. Cladding of aluminum on AISI 304L stainless steel by cold roll bonding: Mechanism, microstructure, and mechanical properties. Mat Sci Eng A-struct. 2014;613:232–9.

[16] Park K, Kim D, Kim K, Kwon H. Aluminum/stainless steel clad materials fabricated via spark plasma sintering. Materials. 2020;13(1):1–10.

[17] Shan LY, Yang L, Wang YP. Improving the high temperature mechanical performance of Cu–Cr alloy induced by residual nano-sized Cr precipitates. Mat Sci Eng A-struct. 2022;845:1–8.

[18] Watanabe C, Monzen R, Tazaki K. Mechanical properties of Cu–Cr system alloys with and without Zr and Ag. J Mater Sci. 2008;43(3):813–9.

[19] Shen DP, Zhu YJ, Yang X, Tong WP. Investigation on the microstructure and properties of Cu–Cr alloy prepared by *in situ* synthesis method. Vacuum. 2018;149:207–13.

[20] Zhang K, Yang JJ, Li JY, Chen XH, Zhou HL, Liu P. Effect of deformation and aging treatment on the microstructure and properties of Cu-0.45Cr-0.14Ti (wt%) alloy. J Alloy Compd. 2021;851:1–8.

[21] Fu SL, Liu P, Chen XH, Zhou HL, Ma FC, Li W, et al. Effect of aging process on the microstructure and properties of Cu–Cr–Ti alloy. Mat Sci Eng A-struct. 2021;802:1–9.

[22] Peng HC, Xie WB, Chen HM, Yang B. Effect of micro-alloying element Ti on mechanical properties of Cu–Cr alloy. J Alloy Compd. 2021;852:1–9.

[23] Pan TJ, Chen J, He YX, Wei W, Hu J. Influence of grain refinement on oxidation behavior of two-phase Cu–Cr alloys at 973–1,073 K in air. High Temp Mat Pr-isr. 2016;35(10):1005–11.

[24] Chen F, Yan ZQ, Wang T. Effects of internal oxidation methods on microstructures and properties of Al_2O_3 dispersion-strengthened copper alloys. High Perform Structl Mater. 2018;1–8.

[25] Guo XH, Zhou YJ, Song KX, Ang X, Liang SH. Microstructure and properties of Cu–Mg alloy treated by internal oxidation. Mater Sci Tech. 2018;34(6):648–53.

[26] Wang H, Gong LK, Liao JF, Chen HM, Xie WB, Yang B. Retaining meta-stable fcc-Cr phase by restraining nucleation of equilibrium bcc-Cr phase in CuCrZrTi alloys during ageing. J Alloy Compd. 2018;749:140–5.
[27] Markandeya R, Nagarjuna S, Sarma DS. Precipitation hardening of Cu-Ti-Cr alloys. Mat Sci Eng A-struct. 2004;371(1–2):291–305.
[28] Shojaeepour F, Abachi P, Purazran KG, Moghanian AH. Production and properties of Cu/Cr_2O_3 nano-composites. Powder Technol. 2012;222:80–4.
[29] Liang SH, Wang XH, Kong DM, Fan ZK. Preparation of Cu/Cr_2O_3 composites by mechanical activation and *in situ* oxidation. J Compos Mater. 2009;44(9):1049–60.
[30] Liang SH, Fang L, Fan ZK. Internal oxidation of Cr in Cu–Cr/Cu_2O composite powder prepared by mechanical activation. Mat Sci Eng A-struct. 2004;374(1):27–33.
[31] Khlebnikova YV, Suaridze TR, Egorova LY, Rodionov DP. Internal oxidation of textured thin tapes of binary copper-based alloys. Phys Met Metallog. 2018;119(11):1107–13.
[32] Smallman RE, Ngan AHW. Chapter 7-Mechanical properties II-Strengthening and toughening. In: Smallman RE, Ngan AHW, editors. Physical metallurgy and advanced materials engineering. 7th edn. Oxford: Butterworth-Heinemann; 2007. p. 385–446.
[33] Pan ZH. Preparation and properties of Cu-Gd_2O_3 gradient composite materials. Qinhuangdao: Yanshan University; 2018.
[34] Li JS, Wang SZ, Mao QZ, Huang ZW, Li YS. Soft/hard copper/bronze laminates with superior mechanical properties. Mat Sci Eng A-struct. 2019;756:213–8.
[35] Yin Z, Yang XC, Ma XL, Moering J, Yang J, Gong YL, et al. Strength and ductility of gradient structured copper obtained by surface mechanical attrition treatment. Mater Des. 2016;105:89–95.
[36] Fu GY, Niu Y, Gesmundo F. Microstructural effects on the high temperature oxidation of two-phase Cu–Cr alloys in 1 atm O_2. Corros Sci. 2003;45(3):559–74.
[37] Krishna SC, Rao GS, Jha AK, Pant B, Venkitakrishnan PV. Strengthening in high strength Cu–Cr–Zr–Ti alloy plates produced by hot rolling. Mat Sci Eng A-struct. 2016;674:164–70.
[38] Dai J, Ma MZ, Xiao Z, Meng XP, Sun G, Zhang TY, et al. Effect of trace silicon addition on microstructure and properties of a Cu–0.26Cr–0.14Mg alloy. Mat Sci Eng A-struct. 2022;833:1–11.